ACS APPLIED MATERIALS & INTERFACES

Research Article

www.acsami.org

Interfacial Processes and Influence of Composite Cathode Microstructure Controlling the Performance of All-Solid-State Lithium Batteries

Wenbo Zhang,[†] Dominik A. Weber,[†] Harald Weigand,[†] Tobias Arlt,[‡] Ingo Manke,[‡] Daniel Schröder,[†] Raimund Koerver,[†] Thomas Leichtweiss,[†] Pascal Hartmann,[§,∥] Wolfgang G. Zeier,*[,†] and Jürgen Janek*[,†,∥]

[†]Physikalisch-Chemisches Institut, Justus-Liebig-Universität Giessen, Heinrich-Buff-Ring 17, 35392 Giessen, Germany

[‡]Helmholtz-Zentrum Berlin für Materialien und Energie GmbH, Hahn-Meitner-Platz 1, 14109 Berlin, Germany

[§]BASF SE, 67056 Ludwigshafen am Rhein, Germany

[∥]BELLA, Institut für Nanotechnologie, Karlsruher Institut für Technologie, Hermann-von-Helmholtz-Platz 1, 76344 Eggenstein-Leopoldshafen, Germany

Supporting Information

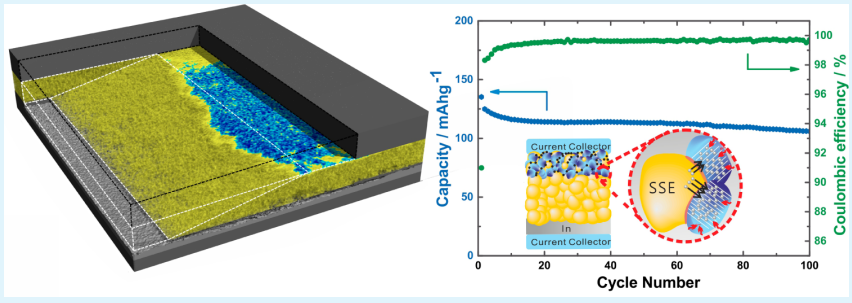

ABSTRACT: All-solid-state lithium-ion batteries have the potential to become an important class of next-generation electrochemical energy storage devices. However, for achieving competitive performance, a better understanding of the interfacial processes at the electrodes is necessary for optimized electrode compositions to be developed. In this work, the interfacial processes between the solid electrolyte ($Li_{10}GeP_2S_{12}$) and the electrode materials (In/InLi and Li_xCoO_2) are monitored using impedance spectroscopy and galvanostatic cycling, showing a large resistance contribution and kinetic hindrance at the metal anode. The effect of different fractions of the solid electrolyte in the composite cathodes on the rate performance is tested. The results demonstrate the necessity of a carefully designed composite microstructure depending on the desired applications of an all-solid-state battery. While a relatively low mass fraction of solid electrolyte is sufficient for high energy density, a higher fraction of solid electrolyte is required for high power density.

KEYWORDS: *SSB, all-solid-state batteries, $Li_{10}GeP_2S_{12}$, electrochemical energy storage, solid electrolyte*

1. INTRODUCTION

Rechargeable Li-ion batteries with liquid electrolytes have become the most important mobile energy storage devices for consumer applications, and they will play a similar key role in electric vehicles.[1] The classic "rocking chair" lithium-ion battery (LIB) includes layered lithium storage compounds, graphite, and transition metal oxides, as anode and as cathode, respectively. Li ions are exchanged between the two electrodes during charging and discharging and transported by the purely ion-conducting liquid electrolyte (LE). While this concept obviously works very well and has been continuously improved by a factor of 4 in energy density during the last 25 years, a limit will be approached soon.[2] In addition, some disadvantages are inherently connected to the use of liquid electrolytes, which are composed of organic carbonates as solvents and $LiPF_6$ as a conducting salt. The limited electrochemical stability of the liquid electrolytes determines the maximum operating voltage of lithium-ion batteries, and cathode instabilities lead to capacity fading.[3] The anode forms a solid electrolyte interphase (SEI); gaseous compounds are formed by side reactions at both electrodes.[4,5] Potential threats in extreme cases can occur due to the electrolyte flammability.[3,6] In addition, liquid electrolytes allow for the dissolution of active species such as Mn or Ni ions at the cathode and their diffusion to the anode. This unwanted

Received: January 23, 2017
Accepted: May 8, 2017
Published: May 8, 2017

ACS Publications © 2017 American Chemical Society

DOI: 10.1021/acsami.7b01137
ACS Appl. Mater. Interfaces 2017, 9, 17835−17845

Ningde Amperex Tech. Exhibit No. 2023
Zhuhai CosMX Battery Co. Ltd. v. Ningde Amperex Tech.
IPR2025-00722, U.S. Patent No. 11,799,131
Page 1 of 11

"chemical cross-talk" between the electrodes further impedes the long-term cyclability of lithium-ion batteries in high-voltage systems.[7] For large-scale energy storage systems such as electric vehicles, reliable and robust battery systems are necessary. Next-generation solid-state batteries (SSB), without liquid electrolytes, are now considered as a promising next-generation technology beyond LIB.[8] The substitution of the liquid electrolyte for an inorganic solid electrolyte (SE) may not only enhance the safety but also enlarge the operating voltages within a battery, in turn leading to significantly larger energy densities for the whole system altogether, if a lithium metal electrode is used.[2,9,10]

The performance of a SSB strongly depends on the type of SE, its compatibility to the active materials, the mechanical softness and elasticity of the SE/active materials composite, as well as the particle distribution throughout the cathode.[11] In particular, the elasticity of the SE is vital for a good cycling behavior of the cell because the volume changes of the active materials may lead to electrode cracking and loss of contact between the particles.[12] Sulfides and thiophosphates show sufficiently high ionic conductivities to replace liquid electrolytes[13−15] and, in addition, exhibit good mechanical properties due to their low Young's moduli.[12,16] As the Young's modulus is a reflection of mechanical softness and elasticity of the sulfide electrolyte, a softer electrolyte enables consolidation at room temperature and more intimate particle contact. In comparison, oxide SE are usually mechanically quite rigid and stiff[17] but offer good solid-state performance if porous networks are used.[18] The interfacial resistances for the Li^+ transfer between the active material and the solid electrolyte need to be low in order to reduce the corresponding overpotential. In addition, chemical stability of the solid electrolyte against the anode and the cathode is paramount.[19] While the thermodynamic instability against lithium metal as an anode material has recently been demonstrated for most solid electrolytes,[19−24] less is known for the stability of solid electrolytes at the cathode side.[25,26] A large Li^+ transfer resistance occurs when sulfide solid electrolytes are in direct contact with cathode active materials, possibly due to a resistive layer from the mutual interdiffusion between the active material and the electrolyte and the formation of blocking reaction products.[26] A strategy to suppress the highly resistive layer is to insert a buffer layer between the sulfide SE and the oxide active material. Ideally, amorphous and very thin buffer layers are used to keep the interfacial resistance small.[27−29]

In addition to the modification of the interface by cathode coating, the design of a three-dimensional composite cathode with optimized transport paths for electrons and ions plays an important role in optimizing the SSB performance. This is similar to using a conventional electrode in which the microstructure and porosity also play an important role for the charge and discharge kinetics in liquid electrolytes.[30] In traditional lithium-ion batteries, the liquid electrolyte penetrates the porous electrodes and provides good contact as well as good ionic percolation pathways. In an all-solid-state battery, however, the solid electrolyte with its specific microstructure and grain distribution may not be in contact with all of the active material. In other words, for a full utilization of the active material sufficient ionic percolation pathways are necessary for shuttling ions between the electrodes, while a good electronic percolation is necessary to transport the electrons to the current collector.

Inspired by the challenges inherent to a "solidified" battery, we investigated the interfacial processes occurring in an all-solid-state battery using state-of-charge- and state-of-discharge-dependent impedance spectroscopy and analyzing the electrochemical cycling behavior. In addition to the interfacial processes, we report on the influence of the mass fraction of the solid electrolyte and the active material in these composite cathodes on the cell performance. Comparing the rate capability, long cycle stability, and interfacial resistances we find that ionic percolation pathways are more important if a high-power solid-state battery is desired, whereas for high-energy batteries the electronic percolation appears to be the more important factor. Depending on the type of application, a specific composite design is important. To our best knowledge, systematic studies on potential-dependent interfacial processes and the influence in composite cathode controlling rate performance have yet not been reported.

2. EXPERIMENTAL SECTION

Synthesis. The solid electrolyte $Li_{10}GeP_2S_{12}$ (LGPS)[14] was synthesized on a solid-state route followed by an annealing step in an ampule under vacuum. Li_2S (Sigma-Aldrich, 99.99%), P_2S_5 (Sigma-Aldrich, 99.99%), GeS (Sigma-Aldrich, 99.99%), and S (Sigma-Aldrich, >99.5%) were used as precursors. In addition, a 5 mol % excess of sulfur was added to the stoichiometric mixture in order to compensate for the loss of sulfur during the annealing process. All precursors were mixed in a planetary ball mill (Fritsch Pulverisette 7) for 24 h at a rotation speed of 500 rpm using ZrO_2 milling balls. An intermediate cooling time (to prevent sample overheating and sulfur evaporation) of 15 min was allowed between 5 min ball mill. Subsequently, the mixed powders were filled into a quartz ampule (1 g per ampule) in an argon glovebox, followed by evacuating and sealing the ampule. Annealing of the powders in the evacuated ampule was conducted for 30 h at 500 °C after applying a heating rate of 27.7 K/h. The crystallized LGPS electrolyte was stored in a glovebox (MBraun) with O_2 and H_2O contents below 0.1 ppm. Laboratory X-ray diffraction was employed to ensure phase purity of LGPS, as has been reported elsewhere.[20] The total conductivity of the synthesized solid electrolyte using blocking gold electrodes was 5 mS/cm. The partial electronic conductivity was determined to be 9 nS/cm in a previous study,[20] i.e., the electronic transference number is about 1.8×10^{-6}.

Surface Coating of $LiCoO_2$. The commercially obtained $LiCoO_2$ (Alfa Aesar, 97%) was surface coated with a $LiNb_{0.5}Ta_{0.5}O_3$ (LNTO) film using a sol−gel route. This composition has recently been identified as promising using a high-throughput method,[31] and the synthesis has been developed in house. Stoichiometric amounts of lithium acetate ($LiCO_2CH_3$, Sigma-Aldrich, 99.99%), niobium(V) ethoxide ($Nb(OCH_2CH_3)_5$, Sigma-Aldrich, 99.95%, trace metals basis), and tantalum(V) butoxide ($Ta(OCH_2CH_2CH_2CH_3)_5$, Sigma-Aldrich, 99.99%, trace metals basis) were dissolved in absolute ethanol (Sigma-Aldrich, >99.8%, GC) and form a homogeneous sol. Then 2 g of powdered $LiCoO_2$ was added to 1 mL of the prepared solution to obtain a coating layer that corresponds to roughly 1.4 wt % of the coated powder. After thoroughly mixing in an ultrasonic bath, the ethanol was removed under vacuum. The remaining wet powders were placed into an oven at 300 °C overnight, followed by a fast annealing step at 450 °C for 1 min. Before fabrication of the SSBs, the coated $LiCoO_2$ powders were dried again in a vacuum (Büchi) oven at 120 °C overnight and afterwards stored in an argon-filled glovebox. X-ray diffraction data for the coated and uncoated $LiCoO_2$ can be found in the Supporting Information. In addition, the influence of the coating in comparison to uncoated $LiCoO_2$ on the electrochemical performance can be found in the Supporting Information.

Cell Assembly. In conventional LIBs, cathodes are prepared by coating the cathode slurry on an Al sheet with about 30% porosity. Carbon is added to the slurry in order to enhance the electronic conductivity of the cathode. In SSB based on sulfide solid electrolytes and $LiCoO_2$, sufficient electron-conducting paths were achieved by

DOI: 10.1021/acsami.7b01137
ACS Appl. Mater. Interfaces 2017, 9, 17835−17845

Ningde Amperex Tech. Exhibit No. 2023
Zhuhai CosMX Battery Co. Ltd. v. Ningde Amperex Tech.
IPR2025-00722, U.S. Patent No. 11,799,131
Page 2 of 11

simply contacting $LiCoO_2$ particles via cold pressing. Upon deintercalation, $LiCoO_2$ changes from semiconducting to metallic character, which further improves the electronic conductivity.[32] Thus, in the present work, all composite cathodes were prepared without carbon as additive. The SSBs were constructed in a homemade cell casing, which is shown in the Supporting Information. When assembling the cell, one side of the current collector was kept closed while the other side was left open. An 80 mg amount of the solid electrolyte powder was first added into the PEEK (polyether ether ketone) cylinder and hand pressed into a pellet form. The inner wall of the PEEK cylinder has a diameter of 10 mm. The composite cathode was prepared by hand mixing $LiCoO_2$ and LGPS in different mass ratios (40:60, 50:50, 60:40, 70:30, and 80:20, corresponding to volume ratios of 21:79, 29:71, 38:62, 49:51, and 62:38, respectively) in an agate mortar for 15 min. A 10 mg amount of this mixed powder was homogeneously distributed on one side of the preformed solid electrolyte pellet, followed by uniaxial pressing with 3.5 t for 2 min. After the first pressing step, a thin indium foil with an 8 mm diameter (Alfa Aesar, 99.99%, 0.125 mm thickness) serving as the anode was added to the other side of SE pellet and pressed with 1.5 t for 2 min. Afterwards, constant pressure was applied to the cell using the screw (Supporting Information Figure S3) of the aluminum framework with 10 N m torque, which was kept constant during the electrochemical tests. In the case of long-term cycling, an additional thin Li foil was attached to the indium foil with a weight ratio of 1:60 in order to compensate for lithium loss over time.

Electrochemical Tests. Different electrochemical measurements were conducted with the above-mentioned battery cells. Galvanostatic cycling of the cells was carried out in the voltage range from 2.0 to 3.6 V vs In/InLi. Here, the In/InLi is used to represent the lithiated indium anode. The In/InLi anode itself exhibits a constant potential of about 0.6 V against Li/Li^+, i.e., the potential range corresponds to about 2.6−4.2 V[33] against Li/Li^+. The theoretical capacity of $LiCoO_2$ was taken as 137 mAh/g, calculated based on $Li_{0.5}CoO_2$ in the fully charged state.[34] The C rate was calculated based on the weight of the pure $LiCoO_2$ in the composite cathode. Rate tests were performed in order to probe how electronic and ionic paths influence the rate performance and long cycle stability of the SSB. In the performed rate-capability tests, the cells were charged with 0.05 C and discharged at different C rates, from 0.1 to 10 C. For instance, 1 C corresponds to 1.045 mA/cm^2 in the cell with 7.64 mg/cm^2 $LiCoO_2$ as active material. In addition, cyclic voltammetry (CV) measurements were conducted in the same voltage range as the galvanostatic cycling using a scan rate of 0.02 mV/s. For all tests we used the VMP3 electrochemical workstation by Bio-Logic Science Instruments SAS.

Electrochemical impedance spectroscopy (EIS) was carried out using the SP300 electrochemical workstation by Bio-Logic Science Instruments SAS after charging the cells to 3.6 V vs In/InLi at 0.1 C, followed by a rest period of 30 min. An excitation voltage of 10 mV was chosen for measurements in the frequency range from 7 MHz to 10 mHz with 10 points per decade.

Scanning Electron Microscopy. Cross-sectional and top-view micrographs of disassembled cells were obtained on a Merlin high-resolution scanning electron microscope (Carl Zeiss AG, Germany). The cross section as obtained by carefully breaking the pellet into two pieces inside the glovebox. Energy-dispersive X-ray spectroscopy (EDS) of the composite cathode was carried out using an INCAEnergy detection unit (Oxford instruments) with an acceleration voltage of 10 kV.

Tomography Analysis. A conventional X-ray source was used for full view in situ tomographic measurements of the battery interior. The accelerating voltage was tuned to 80 kV, while the current at the tungsten anode was adjusted to 125 μA. No filter was applied. There were 1200 projections taken for a full tomography (full range over 360°). Each angular step was exposed three times for 1.6 s to increase the signal-to-noise-ratio. The projections were taken using a Hamamatsu flat panel detector with 2316 × 2316 pixel with a pixel size of 50 μm (6.25 μm pixel size in the reconstructed three-dimensional images). For this analysis a special PEEK housing without an aluminum framework, but yet similar to the aforementioned cell casing, was applied (see Supporting Information).

3. RESULTS AND DISCUSSION

In this study, all tests were carried out with the model cell system $In/Li_{10}GeP_2S_{12}/LiCoO_2$. $LiCoO_2$ is chosen because it is well understood as a cathode material in conventional batteries and a potential candidate in SSB due to its favorable electronic transport properties.[11,35] The surface of $LiCoO_2$ was coated with $LiNb_{0.5}Ta_{0.5}O_3$ as a protective layer for preventing side reactions.[27,31] $Li_{10}GeP_2S_{12}$ was employed due to its high Li^+ conductivity which is comparable to the conductivity of liquid electrolytes.[14] In order to avoid any possible side reactions between SE and Li metal, indium metal is used as anode, which presents a stable potential of about +0.6 V against Li/Li^+.[33,36]

Microstructure of the Solid-State Batteries. Figure 1a shows a scanning electron microscopy (SEM) micrograph of

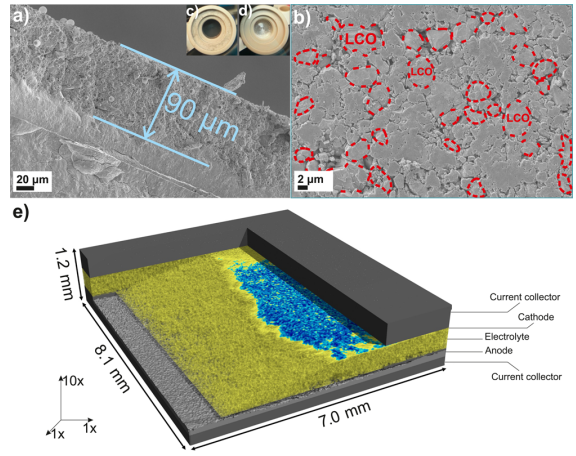

Figure 1. (a) Scanning electron micrograph (SEM) in a cross-sectional view of the all-solid-state composite cathode and $Li_{10}GeP_2S_{12}$ solid electrolyte. Thickness of the composite cathode is around 90 μm. (b) SEM top view of the SSB composite cathode (m($LiCoO_2$):m(LGPS) = 70:30). Some of the active material $LiCoO_2$ is highlighted using red broken lines. (c) Photo taken from the composite cathode side. Homogeneous distribution of the composite cathode is achieved. (d) Photo taken from the indium anode side. Indium foil completely covers the SE pellet after cold pressing. (e) 3D reconstruction of the X-ray tomography of a cold-pressed all-solid-state battery, showing the thicknesses of the different layers within the cell.

the composite cathode (m($LiCoO_2$):m(LGPS) = 70:30) corroborating good physical mixing of the active material and the solid electrolyte powders. In addition, the composite cathode appears quite dense, and good contact between the composite cathode and the SE membrane is obtained, which has been prepared by uniaxial cold pressing. As Young's moduli reflect softness and elasticity of the materials, the good densification behavior can be attributed to the low Young's Modulus of the sulfide solid electrolyte of about 10.5 GPa.[16] From the cross-sectional view the thickness of the composite cathode can be estimated to be roughly 90 μm. As the image was taken after disassembling the cell, the actual thickness of the composite cathode during operation must be thinner than 90 μm, taking into account the constantly applied uniaxial pressure on the current collectors during operation. The solid electrolyte membrane itself appears quite dense, and no

DOI: 10.1021/acsami.7b01137
ACS Appl. Mater. Interfaces 2017, 9, 17835−17845

Ningde Amperex Tech. Exhibit No. 2023
Zhuhai CosMX Battery Co. Ltd. v. Ningde Amperex Tech.
IPR2025-00722, U.S. Patent No. 11,799,131
Page 3 of 11

obvious pores are visible in the SEM micrograph. Minor cracks can be observed that were most likely generated during disassembly of the cell. The $LiCoO_2$ particles at the side of the current collector (red highlighted areas of Figure 1b) are not fully covered by $Li_{10}GeP_2S_{12}$, which ensures good electronic contact with the current collector. $LiCoO_2$ particles are surrounded by $Li_{10}GeP_2S_{12}$ and well distributed throughout the electrode as seen in the EDX mapping in Figure 2. The insets, Figure 1c and 1d, show photographs of the cathode and anode sides, respectively. After pressing, the cathode side is dark gray due to the mixing of $LiCoO_2$ and $Li_{10}GeP_2S_{12}$ and the anode side is completely covered by the indium foil.

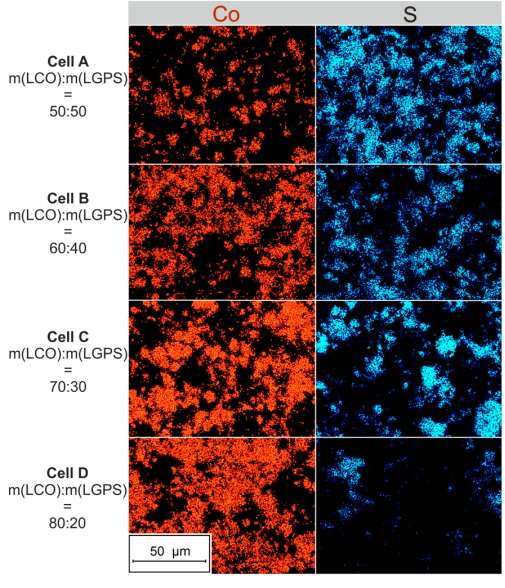

Figure 2. EDX mapping of composite cathodes of cells A−D representing different cathode compositions. Co is shown in orange and S in blue. In cell A, most of the $LiCoO_2$ particles are separated by the solid electrolyte. From cell B to D, more overlap between $LiCoO_2$ particles can be observed, which creates more electronic-conducting paths but also extends the average Li^+ diffusion length (see Figure 8). In cell D, the contact area between $LiCoO_2$ and $Li_{10}GeP_2S_{12}$ is limited, which restricts Li^+ conductivity. Cells B and C show a much more balanced and homogeneous distribution of $LiCoO_2$ and $Li_{10}GeP_2S_{12}$, which is the basis for good electrochemical performance.

In order to understand the effects of the composite cathode composition on the rate performance of all-solid-state batteries, mixtures with different mass fractions of active material and SE were prepared. The distribution of $LiCoO_2$ and $Li_{10}GeP_2S_{12}$ in the composite cathode of different cells is shown in the elemental energy-dispersive X-ray spectroscopic maps for Co and S (see Figure 2). The elemental emission lines of Co and S were chosen to represent the distribution of $LiCoO_2$ and $Li_{10}GeP_2S_{12}$, respectively.

Figure 1e shows an in situ recorded X-ray tomographic image of a cold-pressed pellet of the here-assembled all-solid-state battery. While the layer thicknesses may differ slightly from cell to cell, the amount of starting materials (10 mg of composite cathode ($m(LiCoO_2)$:m(LGPS) = 70:30), 80 mg of LGPS as membrane) and surface areas were kept constant. Employing the tomography data, a thickness of the solid electrolyte separator of ∼600 μm is observed. These values correspond well with the thicknesses obtained via scanning electron microscopy of a postmortem cell and the thicknesses calculated based on impedance spectroscopy data (see the next section).

Electrochemical Performance of Solid-State Batteries. As recently reported, a coating layer leads to positive effects on the cell performance, especially to an increase in rate capability and capacity retention.[27,37] This has been mainly attributed to the decrease of the interfacial resistance between the layered cathode phases Li_xMO_2 and the solid electrolytes,[26,27] as well as to the possible prevention of interfacial reactions[38] (which may as well cause an additional increase in the interfacial resistances). Recently, a highly conductive Li−Nb−Ta oxide has been identified in a high-throughput approach and reported as an effective coating material.[31] Compared to $LiNbO_3$, this partially crystallized Li−Nb−Ta oxide shows an improvement in ionic conductivity as well as in permittivity. On the basis of these results, $LiNb_{0.5}Ta_{0.5}O_3$ (LNTO) was implemented as an amorphous interlayer in the present work. The impedance response of the all-solid-state cells with LNTO-coated $LiCoO_2$ was recorded after charging to 3.6 V vs the In/InLi electrode (current density of 0.1 C). A comparison to the uncoated $LiCoO_2$ can be found in the Supporting Information. Two semicircles located in the midfrequency region (from 1 kHz to 100 Hz) and low-frequency region (∼1 Hz) are observed. The resistance of the solid electrolyte ($R_{SE,bulk}$) is about 15 Ω for both samples, corresponding well to the electrolyte thickness of roughly 590 μm, based on the conductivity of the solid electrolyte of 5 mS/cm. A purely resistive contribution, representing the bulk resistance of the solid electrolyte separator layer at the high-frequency region (>1 MHz) is visible. In addition, a very small resistance ($R_{HF} \approx 2$ Ohms), which we attribute to the grain boundary resistance of the cold-pressed $Li_{10}GeP_2S_{12}$ solid electrolyte, is observed around 518 kHz and a capacitance of 0.79 μF. The semicircle in the low-frequency region (with R_{LF}) is assigned to the interface between the negative electrode indium layer and the solid electrolyte, corresponding well with the results observed in other reports.[32,33] A capacitance value of 7.64 mF is obtained after fitting this process. These data suggest that the oxide coating effectively suppresses the formation of a highly resistive interface and supports the Li^+ transport across this interface (see Supporting Information). While Nyquist plots obtained in conventional liquid-electrolyte lithium-ion batteries with $LiCoO_2$ usually show semicircles that can be related to charge transfer resistances and the electronic properties of the active material, only one semicircle in the midfrequency range is observed in SSB. This observance is due to the proximity of the time constants related to the underlying transport processes. Alternatively, it could be due to interphase formation dominating the transfer of Li^+. In both cases, a Warburg region at very low frequency is observed. This Warburg-type impedance can be attributed to the solid-state Li^+ diffusion inside $LiCoO_2$ particles.[40,41]

Galvanostatic charge−discharge curves (Figure 3b) and cyclic voltammetry (CV) measurements (Supporting Information Figure S5) are used to show the well-running behavior of the SSB. The initial charge capacity of 136 mAh/g can be obtained with only a small overpotential for both charge and discharge curves. The first cycle efficiency amounts to 91.1%. At the end of the charge curve of the cell, a small increase of the potential occurs, corresponding to the typical phase transition from hexagonal to monoclinic at 3.46 V vs In/InLi (4.08 V vs

DOI: 10.1021/acsami.7b01137
ACS Appl. Mater. Interfaces 2017, 9, 17835−17845

Ningde Amperex Tech. Exhibit No. 2023
Zhuhai CosMX Battery Co. Ltd. v. Ningde Amperex Tech.
IPR2025-00722, U.S. Patent No. 11,799,131
Page 4 of 11

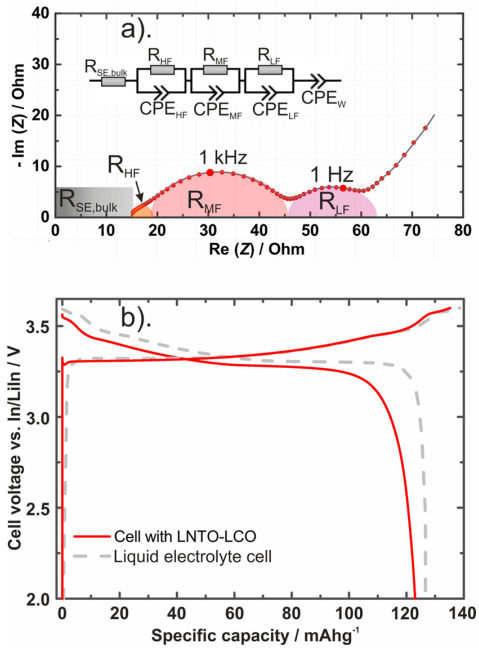

Figure 3. (a) Nyquist plots for SSBs after the initial charge with LNTO-coated $LiCoO_2$. Equivalent circuit R(RQ) (RQ) (RQ)Q is used for the fitting (Q is a constant phase element, CPE, which represents an imperfect capacitor). Spectra were recorded in the frequency range from 7 MHz to 10 mHz. The subscripts HF, MF, and LF represent high-frequency, midfrequency, and low-frequency, respectively. Tail at low frequency could be attributed to a Warburg region, which is characterized by a ~45° angle to the real axis. Warburg region can be assigned to the solid-state diffusion of Li^+ inside $LiCoO_2$ particles. Detailed fitting parameters are listed in the Supporting Information. (b) Charge−discharge curves of SSB with LNTO-coated $LiCoO_2$ (red curves). Charge−discharge curves of $LiCoO_2$ in liquid electrolyte as comparison is also shown in gray. All-solid-state cells are cycled at 0.1 C (115 $\mu A/cm^2$).

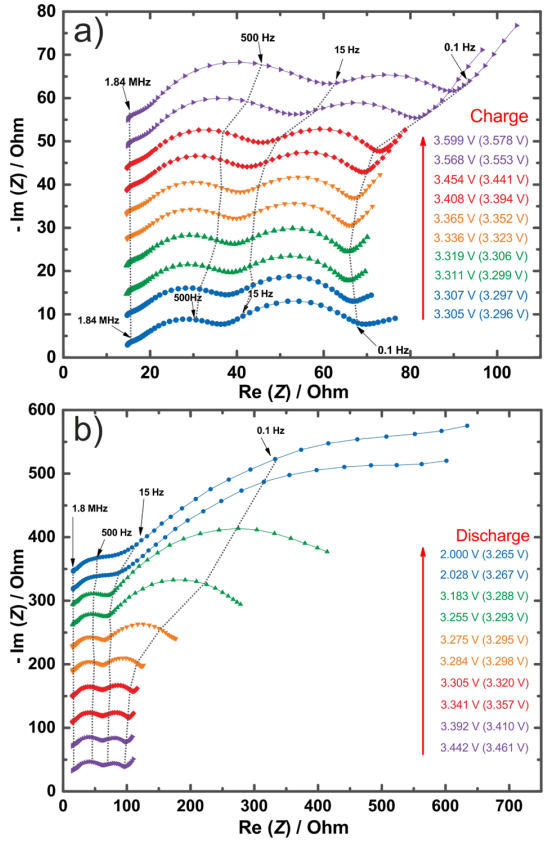

Figure 4. Stacked Nyquist plots of SSB with LNTO-coated $LiCoO_2$ as active material during (a) the charge and (b) the discharge process. Galvanostatic charge was carried out at 0.1 C, and EIS was carried out after 1 h charge and 30 min rest. Given potential values denote the potential after the galvanostatic process. In parentheses the OCV after 30 min rest and at which the impedance measurements were carried out is given. R(RQ) (RQ) (RQ)Q equivalent circuit is employed for the fitting. While in the charge process the interfacial resistance between the solid electrolyte and the coating appears to increase, the major impedance increase in the discharge can be related to the interface between the electrolyte and the indium anode. As depicted in Figure 3, a Warburg impedance at very low frequency forms with the increase of SOC, indicating the solid-state Li^+ diffusion in $LiCoO_2$.

Li^+/Li) and from monoclinic back to hexagonal at 3.58 V versus In/InLi (4.2 V vs Li^+/Li).[34] This is further visible in the cyclic voltammograms shown in Supporting Information Figure S5. Besides the two small peaks at high voltage, two main peaks at 3.36 and 3.25 V are recorded that correspond well to the first-order transition of $LiCoO_2$ during deintercalation and intercalation.[34] The discharge curve of the all-solid-state cell shows a lower voltage compared to the liquid cell,[42] due to the relatively lower ionic conductivity of LGPS compared to the liquid electrolyte and a therefore resulting in some additional overpotential. However, the electrochemical performance is comparable to that of liquid electrolyte cells, showing satisfying performance of the all-solid-state cell when a coated $LiCoO_2$ is used.

Interfacial Processes in the Solid-State Batteries. For the purpose of monitoring interfacial resistance contributions, the changes in the impedance spectra, depending on the state-of-charge (SOC) and state-of-discharge (SOD), are conducted. The obtained impedance responses are shown in Figure 4a and 4b, and the corresponding resistance contributions, obtained via fitting the impedance data, are shown in Figure 5. Two semicircles are observed in all spectra taken at different potentials during the charge process. Starting with a "fresh" cell, only a virtually linear response starting from about 20 Ω is observed (Supporting Information Figure S10). Two semicircles appear once the voltage approaches 3.3 V (vs In/InLi) during the initial charge. A drop of the initial resistance from 20 to 17 ohm is observed after charging to 3.3 V, which closely relates to the consolidation of solid electrolyte. The pressure change of the model SSB during cycling has been in situ observed, and the results are shown in another paper from our group.[43] In the charging process, the low-frequency semicircle—corresponding to the In/SE interface—remains almost unchanged once it is formed. Interestingly, the midfrequency semicircle, and with it the interfacial resistance, related to the cathode/SE interface, increases slowly with increasing potential. This is quite different compared to the EIS spectra of $LiCoO_2$ in liquid electrolyte cells.[41] In liquid electrolyte cells, the high-frequency semicircle representing the SEI layer on $LiCoO_2$ remains stable with changing charge potential once it is formed.

DOI: 10.1021/acsami.7b01137
ACS Appl. Mater. Interfaces 2017, 9, 17835−17845

Ningde Amperex Tech. Exhibit No. 2023
Zhuhai CosMX Battery Co. Ltd. v. Ningde Amperex Tech.
IPR2025-00722, U.S. Patent No. 11,799,131
Page 5 of 11

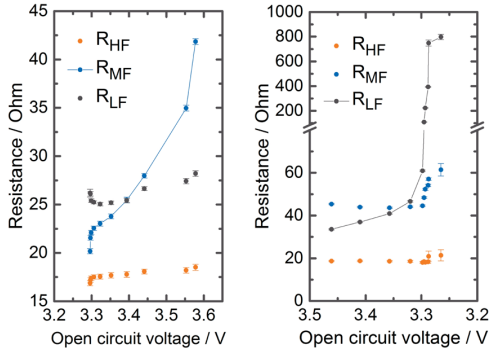

Figure 5. Summary of EIS results of SSB with LNTO-coated $LiCoO_2$ as active material. Potential dependence of the resistance of SE (R_{HF}) (including bulk and grain boundary contributions) of the interface between the cathode and the SE (R_{MF}) and of interface between In and SE (R_{LF}): (left) During charge and (right) discharge process.

The midfrequency semicircle corresponding to electrical properties of $LiCoO_2$ decreases with the increase in charge potential, owing to the change in properties of $LiCoO_2$ from semiconductor to metal during Li deintercalation.[41,44] In the case of the SSB, the increase of the interfacial resistance between the cathode material and the solid electrolyte with charging potential can be attributed to the following factor.

The amorphous coating represents a thin layer (<10 nm, 1 wt %), and certain local regions of the coating on the surface of $LiCoO_2$ may break apart as a result of the anisotropic volume expansion of $LiCoO_2$ (i.e., ~2% volume expansion in the *c* direction up to $Li_{0.5}CoO_2$ during delithiation).[34] Any cracks formed on the coating layer would interrupt the continuous Li^+ percolation paths, leading to local contact loss and contributing to the increase in interfacial resistance. In addition, the increased cell potential may lead to severe decomposition of $Li_{10}GeP_2S_{12}$ because the electrochemical window of LGPS is quite narrow (1.7−2.14 V vs Li/Li^+).[22,45,46] The oxidation of the sulfide-based electrolyte has been corroborated using X-ray photoemission, as shown in Supporting Information Figure S13. Consequentially, the interfacial resistance would increase with the accumulation of side products during the charge process, due to the poor Li^+ conductivity of these side products.[19,22] Noticeably, the interfacial resistance increases at the end of the charging process by a factor of about 2. One of the reasons is the relatively large volume expansion during the transition between the hexagonal and the monoclinic phase. If the cracking of the electrodes indeed occurs, one could expect deterioration of the long-term cycle stability of the all-solid-state battery. In addition to poorly conducting side phases, these decomposition products will have different mechanical properties as the sulfide-based solid electrolyte and may therefore not be elastic enough to compensate for the volume expansion brought by the delithiation of $LiCoO_2$. When side products accumulate and expand at the interface with the increasing state-of-charge, local contact loss between coated $LiCoO_2$ and SE may occur, possibly resulting in the increase of interfacial resistance with increasing SOC.

In addition to the changing interfacial resistance, in the very low frequency region a noticeable Warburg impedance forms with increasing SOC. A very similar effect has been reported by Levi et al. for LE-LIB.[41] Such Warburg impedance may be assigned to the chemical diffusion of Li in the $LiCoO_2$ particles. The Warburg impedance is larger at high SOC and appears not to contribute at lower SOC. As the chemical diffusion coefficient of Li in LCO increases with SOC,[34] this is somehow counterintuitive. A detailed and more thorough evaluation of the underlying diffusion processes requires measurements at lower frequencies, which will be part of future experiments

Upon discharge, the interfacial resistance between the cathode and the solid electrolyte remains constant until roughly 50% of the discharge capacity is reached, followed by a minor increase, which might simply be a fitting artifact that is brought about by the large increase of the semicircle in the low-frequency region. More obvious, the interfacial resistance between In/SE increases once the discharge begins and reaches almost 800 Ω in the end of the discharge. Such a drastic increase of the resistance indicates that the In/SE interface kinetics strongly depends on the amount of Li in the two-phase In and InLi alloy.[39] The In/SE interfacial resistance increases when the Li to In molar ratio becomes smaller. The large In/SE interfacial resistance at the end of discharge indicates an increased transfer barrier at the interface and results in an irreversible capacity loss. This is one of the reasons for the relative low first cycle efficiency of the SSB and ultimately shows the kinetic problems when using metal electrodes in SSBs.[2] In both charge and discharge processes, the resistance of the solid electrolyte shows no significant change corroborating the stability of the bulk solid electrolyte material itself.

For a more reliable interpretation of the different impedance contributions, the potential-dependent capacities were evaluated and are shown in Figure 6. The very small semicircle

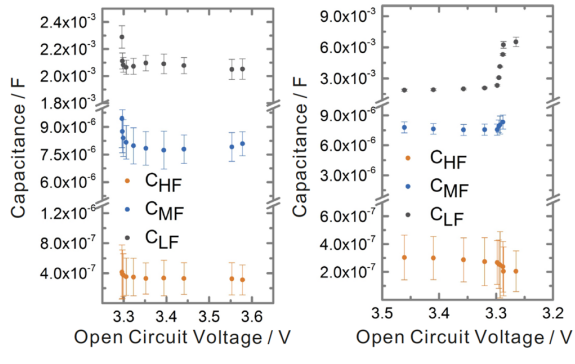

Figure 6. Summary of capacitance data of SSB with LNTO-coated $LiCoO_2$ as active material at different state-of-charge (left) and state-of-discharge (right). Due to the depressed semicircles shown in EIS, constant phase elements (CPEs) were applied for the equivalent circuit and used for the fitting to the measured impedance data. Real capacities were derived from the CPEs (see the derivative processes and error analysis in the Supporting Information).

shown at high frequencies (as shown in Figure 3) is described by a capacity of about 0.3 μF, which corresponds well with the grain boundary capacity of ceramic solid electrolytes.[47] A slightly higher capacity of 6−9 μF is observed for the cathode/SE interface. The highest capacitance in the mF range is attributed to the In/SE interface, which indicates there are narrow contacting "necks" leading to rapid voltage drop between the SE and indium. A decrease in capacity is observed at the initial charging state for all three processes, indicating the cell is becoming geometrically consolidated when the charge begins. This phenomenon has been observed by in situ

DOI: 10.1021/acsami.7b01137
ACS Appl. Mater. Interfaces 2017, 9, 17835−17845

Ningde Amperex Tech. Exhibit No. 2023
Zhuhai CosMX Battery Co. Ltd. v. Ningde Amperex Tech.
IPR2025-00722, U.S. Patent No. 11,799,131
Page 6 of 11

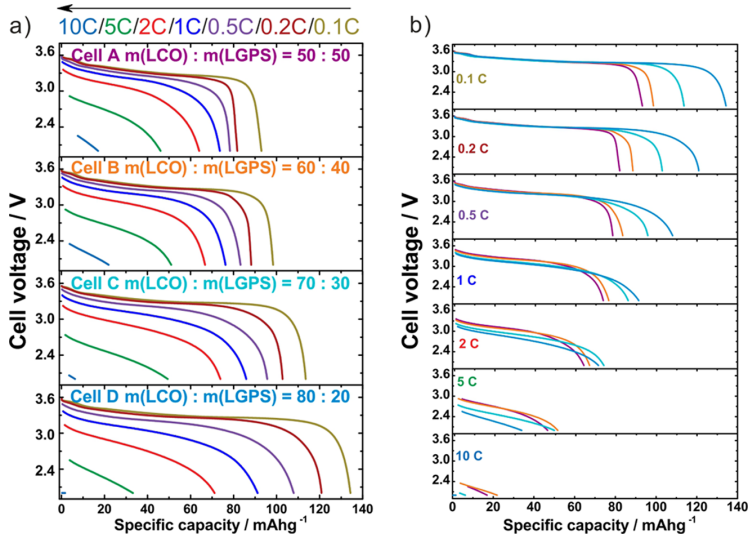

Figure 7. Discharge curves of SSBs with different mass ratios ranging from 50 to 80 wt % of $LiCoO_2$ in the composite cathodes corresponding to cells A–D were shown. All $LiCoO_2$ used in the cells were coated with LNTO. Discharge capacities dependent on C rate are shown in a from right to left; C-rate increases from 0.1 to 10 C. (b) Comparison of discharge curves of cells A–D at different C rates. Overpotential and maximum capacities change with discharging C rate and strongly depend on the ratio between the active material and the solid electrolyte.

monitoring of the pressure change of the SSB and is reported in another work from our group.[43] The consolidation of the SSB is attributed to the volume expansion of both the cathode and the anode materials. The increase in capacitance at the In/SE interface at the end of discharge could be due to the simultaneous increase in the interfacial resistance at a low Li to In mole ratio and the large volume shrinkage when cubic $InLi_{1-x}$ to tetragonal Li transforms during discharge.[43]

In summary, the resistance of the In/SE interface is a function of the Li concentration in the Li–In alloy and leads to kinetic hindrance at low Li contents. The large resistance of the In/SE interface at the end of discharge is mainly responsible for the relative low first-cycle efficiency in SSB.

Cathode Composition-Dependent Rate Performance. The properties of the composite cathode are considered to be decisive for the overall cell performance. Mizuno et al. reported that the morphology of conductive additives is closely related to the high rate performance of SSBs.[48] Since carbon may evoke more side reactions between $LiCoO_2$ and the solid electrolyte,[49] we used no conductive additives in the composite cathode in the present work. $LiCoO_2$ itself provides sufficient electronic conductivity in the composite cathode. The mass ratio of $LiCoO_2$ and $Li_{10}GeP_2S_{12}$ is altered from smaller to larger values, and its influence on the rate performance and long-term cycle stability are elucidated here. For this analysis, only LNTO-coated $LiCoO_2$ was used. Figure 7 shows the discharge curves of cells labeled A–D, which only differ in the mass ratio of $LiCoO_2$ and SE in the $LiCoO_2/Li_{10}GeP_2S_{12}$ composite cathodes, from 50 to 80 wt % (29–62 vol %) (see Figure 2).

The discharge rates were varied from 0.1 to 10 C (e.g., in cell B, corresponding to current densities of 0.1045–10.45 mA/cm^2). The C rates and capacities are calculated based on the mass of $LiCoO_2$ in the cells. Using a low C rate (up to 2 C), higher discharge capacities are obtained when the mass fraction of $LiCoO_2$ is high. In the case of $m(LiCoO_2)$:m(SE) = 40:60, the discharge capacity is only around 25 mAh/g at 0.1 C, as shown in Supporting Information Figure S9. These data in Figure 7 agree well with the fact that effective electronic conductive paths between particles need to be created by the overlap of $LiCoO_2$ particles. A well-performing SSB, without any additional additive, is obtained once the loading of $LiCoO_2$ is larger than 50 wt % in the composite cathode. Below this value, the $LiCoO_2$ particles are not well connected and only a limited fraction of active material can be utilized. The distribution of $LiCoO_2$ and $Li_{10}GeP_2S_{12}$ in the composite cathode of the different cells can be seen in the elemental energy-dispersive X-ray spectroscopic maps of Co and S, as shown in Figure 2.

A higher loading of the active material $LiCoO_2$ (above 70 wt %) gives reasonable discharge capacities at a low current density due to the increased contact probability between active particles. In other words, the fraction of $LiCoO_2$ particles is high enough to create an electronically conducting percolation network. In consequence, the active material can be fully accessed and used in the electrochemical processes. Therefore, at cycling below 2 C, a small fraction of solid electrolyte (e.g., 20 wt %) appears to be sufficient to ensure Li^+ transport and good battery performance.

However, when the current is increased to 5 C, the discharge capacity of the cell with the largest mass ratio of $LiCoO_2$ to SE decreases to 33 mAh/g, which is much smaller than the others. Additionally, Figure 7b shows that from 2 C on cells C and D exhibit a lower discharge potential as cells A and B. This suggests that a larger overpotential is generated at high currents if there is less solid electrolyte material in the composite cathodes. At 10 C, cells C and D ($m(LiCoO_2)$:m(LGPS) = 70:30 and 80:20, respectively) attain almost no capacity, while a capacity of around 20 mAh/g can be obtained for cells A and B, in which more solid electrolyte material is incorporated. This indicates that when the cells discharge at high current densities, a sufficient electrolyte fraction must be provided in order to create enough ionic paths around $LiCoO_2$ particles and hence ensure fast Li^+ transport, necessary for these high C rates.

DOI: 10.1021/acsami.7b01137
ACS Appl. Mater. Interfaces 2017, 9, 17835–17845

Ningde Amperex Tech. Exhibit No. 2023
Zhuhai CosMX Battery Co. Ltd. v. Ningde Amperex Tech.
IPR2025-00722, U.S. Patent No. 11,799,131
Page 7 of 11

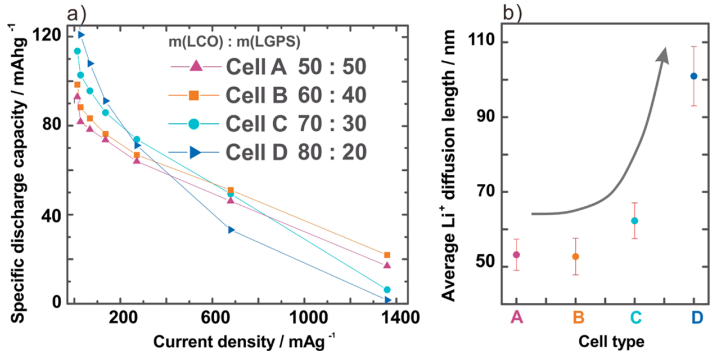

Figure 8. (a) Rate capabilities of cells A–D plotted against current densities. (b) Average Li^+ diffusion length calculated based on the plots in a. Li^+ diffusion coefficient is assumed to be the same for all samples with a value of 1.5×10^{-10} m^2/s.

Impedance spectra of the respective compositions and cells can be found in the Supporting Information, with the smallest interfacial resistance obtained at 70 wt % (cell C). This agrees well with the rate capability test, in which the cell shows a relatively high discharge capacity of up to 5 C. The smaller interfacial resistance indicates a balanced ionic and electronic conductive path when using this ratio.

In addition to the necessary electrolyte fraction, the poor high rate capability of a cell with 80 wt % $LiCoO_2$ may be related to a longer (apparent) Li^+ diffusion length in the active cathode material itself. In order to test this hypothesis, Figure 8a shows the specific discharge capacity plotted against the current density. Such an analysis has been used when analyzing the Li^+ diffusion length for nanocrystalline materials.[50] The dependence of the capacity Q on the current density j results as

$$Q = Q_{1c} - \left(\frac{1}{3}\right)\left(\frac{d^2}{D_{Li}}\right)j \quad (1)$$

with the average diffusion length d of Li ions and the Li diffusion coefficient D_{Li}. It should be noted that this expression only applies strictly under the condition that $Q > 0.5\ Q_{1c}$. Q_{1c} refers to the capacity at 1 C. Employing eq 1, the average Li^+ diffusion length d is proportional to the slope of the Q–j plot under the assumption that all samples have the same diffusion coefficient of Li in $LiCoO_2$, with $D_{Li} = 1.5 \times 10^{-10}$ cm^2/s.[51] In this work, the average Li^+ diffusion length in the composite cathode of cells with different loading of the active material can be approximated based on the fitting of the Q–j plot in the range of $Q > 0.5Q_{1c}$. The results are shown in Figure 8b. As expected, the average Li^+ diffusion length increases from cell A to cell D, corresponding to the fraction of active $LiCoO_2$ material. This suggests that the average Li^+ diffusion length in the composite cathode increases with an increasing fraction of $LiCoO_2$ particles present. In the case of cell D, the large fraction of $LiCoO_2$ particles leads to long percolating pathways while having less contact area with the SE. The average Li^+ diffusion length will be longer in this case than when smaller fractions are used. In other words, longer pathways of diffusion result in the poor high rate capability.

Comparing these results, the importance of proper microstructural design of the composite cathode in all-solid-state batteries becomes evident. The rate capability of a SSB strongly depends on the balance of the electronic and the ionic paths within the composite cathode. On one hand, too much solid electrolyte content prevents sufficient electronic pathways in the active material. On the other hand, too much active material in the composite cathode limits the ionic transport and additionally increases the average Li^+ diffusion length within the network of active storage particles. At low current densities, i.e., slow charge/discharge rates, the electronic pathways appear to be more important and a small fraction of electrolyte is sufficient for complete access of the $LiCoO_2$ particles. At high current densities, more electrolyte is necessary as the cathode particles are only superficially lithiated. Long percolation pathways lower the active surface as well as increase the diffusion path length; both are detrimental to the electrochemical performance. Of course, the results are related to many underlying factors, such as the particle size, mechanical properties of both active material and SE, and/or the incorporation of additives. For example, using nanosized active material may shorten the lithium pathways inside particles and facilitate the rate capability. However, the enhanced surface area may, on the other hand, trigger much more severe decomposition reactions of SE.

In other words, depending on the application of either a high power or a high energy density all-solid-state battery different electrode compositions need to be employed. Further, even more detailed design rules may result from proper microkinetic models of SSB cathodes[48,52]

Cycle Stability. The cycle stabilities of cells A–D were investigated at 0.1 C in the range of 2.0–3.6 V vs In/InLi at room temperature. The results are given in Figure 9. Cell C exhibits the best capacity retention with 70 wt % of $LiCoO_2$ in the cathode, maintaining around 80% of the initial capacity after 100 cycles. Cell B with 60 wt % of $LiCoO_2$ in the cathode also shows comparable performance. The Coulombic efficiency in both cases is above 99.6%, as shown in Figure 9, suggesting minor irreversible reactions in the charge and discharge processes. A higher loading with active material is favorable for obtaining high capacities. It is noteworthy that cell D with the highest $LiCoO_2$ fraction in the composite shows the highest capacity at initial cycles followed by a fast capacity fading. This capacity fade is attributed to the fact that due to the high $LiCoO_2$ fraction, many $LiCoO_2$ particles will have no direct physical contact with the solid electrolyte, resulting in an inhomogeneous distribution of electrochemical reactions at the composite cathode. This hypothesis is strongly supported by a report from Otoyama et al. using Raman spectroscopy for SSB with a high loading of 80 wt % $LiCoO_2$ mixed with a Li_2S–P_2S_5 solid electrolyte.[35] The particles in contact with the solid electrolyte will undergo overcharging within the voltage range

DOI: 10.1021/acsami.7b01137
ACS Appl. Mater. Interfaces 2017, 9, 17835–17845

Ningde Amperex Tech. Exhibit No. 2023
Zhuhai CosMX Battery Co. Ltd. v. Ningde Amperex Tech.
IPR2025-00722, U.S. Patent No. 11,799,131
Page 8 of 11

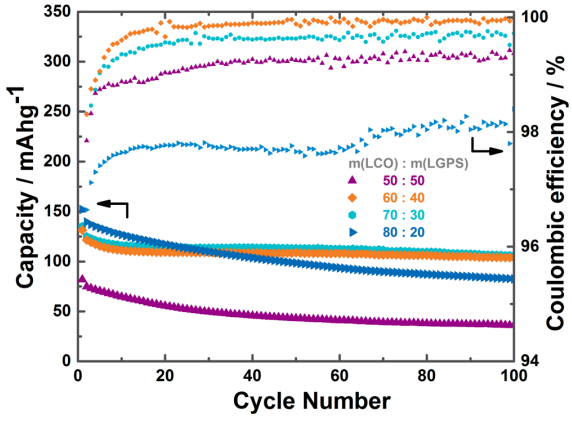

Figure 9. Long cycle performance of cells A–D at a current of 0.1 C. Capacity retention of 80% of the theoretical capacity (137 mAh/g) was achieved with cell C. For all cells, Coulombic efficiency is low for the first cycle, due to formation of interfaces. Cell D shows relatively lower Coulombic efficiency due to the partial overcharge of $LiCoO_2$ in the composite cathode.

(high SOC area), while the other particles cannot be accessed electrochemically due to insufficient contact with the solid electrolyte (low SOC area). The therefore overcharged $LiCoO_2$ will no longer be electrochemical active, which results in capacity fading. In addition, the increase in $LiCoO_2$ mass fraction also increases the effective contact area with SE, which may lead to more decomposition of LGPS at the interface, explaining worse long-term performance. The relative lower Coulombic efficiency (~97.5%) in this case also indicates the loss of electrochemical active material with the process of cycling.

4. CONCLUSIONS

The influence of interfacial transport processes between $LiCoO_2$ and a sulfide solid electrolyte in SSB has been investigated. Using galvanostatic cycling, cyclic voltammetry, and impedance spectroscopy the electrochemical behavior and interfacial resistances were monitored. Without a coating, the interfacial resistance between the solid electrolyte and $LiCoO_2$ cathode material is large and detrimental to the cell performance. Impedance data further show that the volume change during deintercalation increases the interfacial resistance irreversibly. The transfer at the anode interface and the concurrent increase in interfacial resistance between the metal electrode and the solid electrolyte are the reasons for the kinetic hindrance and the relatively low first cycle efficiency of all-solid-state batteries when using metal anodes.

In addition to the investigation of the interfacial processes, the importance of the composite cathode composition has been demonstrated. At low current densities, i.e., slow charge/discharge, good electronic percolation is necessary and a small fraction of the solid electrolyte is sufficient for good electrochemical performance. On the other hand, at high current densities and fast charge/discharge, a higher solid electrolyte fraction is needed in order to electrochemically access all cathode particles fast. In other words, utilization of SSBs as either high-energy or high-power density battery strongly depends on the chosen electrode composition.

■ ASSOCIATED CONTENT

Supporting Information

The Supporting Information is available free of charge on the ACS Publications website at DOI: 10.1021/acsami.7b01137.

Details on the X-ray diffraction data for the coated and uncoated $LiCoO_2$, charge–discharge curves and cyclic voltammetry comparison of a SSB with uncoated $LiCoO_2$, LNTO-$LiCoO_2$ and normal cell in LE, cell casing, SOC/SODC-dependent EIS results with uncoated $LiCoO_2$, charge–discharge curves for a composite electrode with 40 wt % active materia,l and impedance data for the different composite cells (PDF)

■ AUTHOR INFORMATION

Corresponding Authors

*E-mail: wolfgang.g.zeier@phys.chemie.uni-giessen.de.

*E-mail: juergen.janek@phys.chemie.uni-giessen.de.

ORCID

Daniel Schröder: 0000-0002-2198-0218

Wolfgang G. Zeier: 0000-0001-7749-5089

Notes

The authors declare no competing financial interest.

■ ACKNOWLEDGMENTS

We acknowledge financial support within the BASF Scientific Network for Electrochemistry and Batteries. This project was further supported by the Laboratory of Materials Research (LaMa) of JLU. The authors thank Dr. J. Reinacher and Dr. J. Sann for helpful discussion and support. The authors thank Dr. K. Weldert and Dr. B. Mogwitz for help with EDX mapping. The authors thank K. Leitner, J. Kulisch, J. ter Maat, H. Sommer, and A. Schmidt (BELLA Laboratory at INT, Karlsruhe) for helpful discussions and scientific support. Fruitful discussion within the BASF Scientific Network for Electrochemistry and Batteries is highly appreciated.

■ REFERENCES

(1) Tarascon, J. Issues and Challenges Facing Rechargeable Lithium Batteries. *Nature* **2001**, *414*, 359–367.

(2) Janek, J.; Zeier, W. G. A Solid Future for Battery Development. *Nat. Energy* **2016**, *1*, 16141.

(3) Etacheri, V.; Marom, R.; Elazari, R.; Salitra, G.; Aurbach, D. Challenges in the Development of Advanced Li-Ion Batteries: A Review. *Energy Environ. Sci.* **2011**, *4*, 3243.

(4) Michalak, B.; Berkes, B. B.; Sommer, H.; Bergfeldt, T.; Brezesinski, T.; Janek, J. Gas Evolution in $LiNi_{0.5}Mn_{1.5}O_4$/Graphite Cells Studied In Operando by a Combination of Differential Electrochemical Mass Spectrometry, Neutron Imaging, and Pressure Measurements. *Anal. Chem.* **2016**, *88*, 2877–2883.

(5) Imhof, R.; Petr, N. In Situ Investigation of the Electrochemical Reduction of Carbonate Electrolyte Solutions at Graphite Electrodes. *J. Electrochem. Soc.* **1998**, *145*, 1081–1087.

(6) Goodenough, J. B.; Kim, Y. Challenges for Rechargeable Li Batteries. *Chem. Mater.* **2010**, *22*, 587–603.

(7) Michalak, B.; Sommer, H.; Mannes, D.; Kaestner, A.; Brezesinski, T.; Janek, J. Gas Evolution in Operating Lithium-Ion Batteries Studied In Situ by Neutron Imaging. *Sci. Rep.* **2015**, *5*, 15627.

(8) In *Handbook of Solid State Batteries*, 2nd ed.; Feldman, L. C., Eds.; World Scientific Publishing Co. Pte. Ltd.: Singapore, 2015.

(9) Hu, Y.-S. Batteries: Getting Solid. *Nat. Energy* **2016**, *1*, 16042.

(10) Jung, Y. S.; Oh, D. Y.; Nam, Y. J.; Park, K. H. Issues and Challenges for Bulk-Type All-Solid-State Rechargeable Lithium Batteries Using Sulfide Solid Electrolytes. *Isr. J. Chem.* **2015**, *55*, 472.

DOI: 10.1021/acsami.7b01137
ACS Appl. Mater. Interfaces 2017, 9, 17835–17845

Ningde Amperex Tech. Exhibit No. 2023
Zhuhai CosMX Battery Co. Ltd. v. Ningde Amperex Tech.
IPR2025-00722, U.S. Patent No. 11,799,131
Page 9 of 11

(11) Kato, Y.; Hori, S.; Saito, T.; Suzuki, K.; Hirayama, M.; Mitsui, A.; Yonemura, M.; Iba, H.; Kanno, R. High-Power All-Solid-State Batteries Using Sulfide Superionic Conductors. *Nat. Energy* **2016**, *1*, 16030.
(12) Sakuda, A.; Hayashi, A.; Tatsumisago, M. Sulfide Solid Electrolyte with Favorable Mechanical Property for All-Solid-State Lithium Battery. *Sci. Rep.* **2013**, *3*, 2261.
(13) Seino, Y.; Ota, T.; Takada, K.; Hayashi, A.; Tatsumisago, M. A Sulphide Lithium Super Ion Conductor Is Superior to Liquid Ion Conductors for Use in Rechargeable Batteries. *Energy Environ. Sci.* **2014**, *7*, 627−631.
(14) Kamaya, N.; Homma, K.; Yamakawa, Y.; Hirayama, M.; Kanno, R.; Yonemura, M.; Kamiyama, T.; Kato, Y.; Hama, S.; Kawamoto, K.; Mitsui, A. A Lithium Superionic Conductor. *Nat. Mater.* **2011**, *10*, 682−686.
(15) Tatsumisago, M.; Nagao, M.; Hayashi, A. Recent Development of Sulfide Solid Electrolytes and Interfacial Modification for All-Solid-State Rechargeable Lithium Batteries. *J. Asian Ceram. Soc.* **2013**, *1*, 17−25.
(16) Weber, D. A.; Senyshyn, A.; Weldert, K. S.; Wenzel, S.; Zhang, W.; Kaiser, R.; Berendts, S.; Janek, J.; Zeier, W. G. Structural Insights and 3D Diffusion Pathways within the Lithium Superionic Conductor $Li_{10}GeP_2S_{12}$. *Chem. Mater.* **2016**, *28* (16), 5905−5915.
(17) Ni, J. E.; Case, E. D.; Sakamoto, J. S.; Rangasamy, E.; Wolfenstine, J. B. Room Temperature Elastic Moduli and Vickers Hardness of Hot-Pressed LLZO Cubic Garnet. *J. Mater. Sci.* **2012**, *47*, 7978−7985.
(18) Han, X.; Gong, Y.; Fu, K.; He, X.; Hitz, G. T.; Dai, J.; Pearse, A.; Liu, B.; Wang, H.; Rubloff, G.; Mo, Y.; Thangadurai, V.; Wachsman, E. D.; Hu, L. Negating Interfacial Impedance in Garnet-Based Solid-State Li Metal Batteries. *Nat. Mater.* **2016**, *16*, 572.
(19) Richards, W. D.; Miara, L. J.; Wang, Y.; Kim, J. C.; Ceder, G. Interface Stability in Solid-State Batteries. *Chem. Mater.* **2016**, *28*, 266−273.
(20) Wenzel, S.; Randau, S.; Leichtweiß, T.; Weber, D. A.; Sann, J.; Zeier, W. G.; Janek, J. Direct Observation of the Interfacial Instability of the Fast Ionic Conductor $Li_{10}GeP_2S_{12}$ at the Lithium Metal Anode. *Chem. Mater.* **2016**, *28*, 2400−2407.
(21) Hartmann, P.; Leichtweiss, T.; Busche, M. R.; Schneider, M.; Reich, M.; Sann, J.; Adelhelm, P.; Janek, J. Degradation of NASICON-Type Materials in Contact with Lithium Metal: Formation of Mixed Conducting Interphases (MCI) on Solid Electrolytes. *J. Phys. Chem. C* **2013**, *117*, 21064−21074.
(22) Zhu, Y.; He, X.; Mo, Y. First Principles Study on Electrochemical and Chemical Stability of the Solid Electrolyte-Electrode Interfaces in All-Solid-State Li-Ion Batteries. *J. Mater. Chem. A* **2016**, *4*, 3253−3266.
(23) Zhu, Y.; He, X.; Mo, Y. Origin of Outstanding Stability in the Lithium Solid Electrolyte Materials: Insights from Thermodynamic Analyses Based on First-Principles Calculations. *ACS Appl. Mater. Interfaces* **2015**, *7*, 23685−23693.
(24) Hassoun, J.; Verrelli, R.; Reale, P.; Panero, S.; Mariotto, G.; Greenbaum, S.; Scrosati, B. A Structural, Spectroscopic and Electrochemical Study of a Lithium Ion Conducting Li10GeP2S12 Solid Electrolyte. *J. Power Sources* **2013**, *229*, 117−122.
(25) Woo, J. H.; Trevey, J. E.; Cavanagh, a. S.; Choi, Y. S.; Kim, S. C.; George, S. M.; Oh, K. H.; Lee, S.-H. Nanoscale Interface Modification of $LiCoO_2$ by Al_2O_3 Atomic Layer Deposition for Solid-State Li Batteries. *J. Electrochem. Soc.* **2012**, *159*, A1120−A1124.
(26) Sakuda, A.; Hayashi, A.; Tatsumisago, M. Interfacial Observation between $LiCoO_2$ Electrode and $Li_2S-P_2S_5$ Solid Electrolytes of All-Solid-State Lithium Secondary Batteries Using Transmission Electron Microscopy. *Chem. Mater.* **2010**, *22*, 949−956.
(27) Ohta, N.; Takada, K.; Sakaguchi, I.; Zhang, L.; Ma, R.; Fukuda, K.; Osada, M.; Sasaki, T. $LiNbO_3$-Coated $LiCoO_2$ as Cathode Material for All Solid-State Lithium Secondary Batteries. *Electrochem. Commun.* **2007**, *9*, 1486−1490.
(28) Ohta, N.; Takada, K.; Zhang, L.; Ma, R.; Osada, M.; Sasaki, T. Enhancement of the High-Rate Capability of Solid-State Lithium Batteries by Nanoscale Interfacial Modification. *Adv. Mater.* **2006**, *18*, 2226−2229.
(29) Takada, K.; Ohta, N.; Zhang, L.; Fukuda, K.; Sakaguchi, I.; Ma, R.; Osada, M.; Sasaki, T. Interfacial Modification for High-Power Solid-State Lithium Batteries. *Solid State Ionics* **2008**, *179*, 1333−1337.
(30) Okubo, M.; Hosono, E.; Kim, J.; Enomoto, M.; Kojima, N.; Kudo, T.; Zhou, H.; Honma, I. Nanosize Effect on High-Rate Li-Ion Intercalation in $LiCoO_2$ Electrode. *J. Am. Chem. Soc.* **2007**, *129*, 7444−7452.
(31) Yada, C.; Lee, C. E.; Laughman, D.; Hannah, L.; Iba, H.; Hayden, B. E. A High-Throughput Approach Developing Lithium-Niobium-Tantalum Oxides as Electrolyte/Cathode Interlayers for High-Voltage All-Solid-State Lithium Batteries. *J. Electrochem. Soc.* **2015**, *162*, A722−A726.
(32) Ménétrier, M.; Saadoune, I.; Levasseur, S.; Delmas, C. The Insulator-Metal Transition upon Lithium Deintercalation from. *J. Mater. Chem.* **1999**, *9*, 1135−1140.
(33) Takada, K.; Aotani, N.; Iwamoto, K.; Kondo, S. Solid State Lithium Battery with Oxysulfide Glass. *Solid State Ionics* **1996**, *86-88*, 877−882.
(34) Reimers, J. N.; Dahn, J. R. Electrochemical and In Situ X-Ray Diffraction Studies of Lithium Intercalation in Li_xCoO_2. *J. Electrochem. Soc.* **1992**, *139*, 2091.
(35) Otoyama, M.; Ito, Y.; Hayashi, A.; Tatsumisago, M. Raman Imaging for $LiCoO_2$ Composite Positive Electrodes in All-Solid-State Lithium Batteries Using $Li_2S-P_2S_5$ Solid Electrolytes. *J. Power Sources* **2016**, *302*, 419−425.
(36) Webb, S. A.; Baggetto, L.; Bridges, C. A.; Veith, G. M. The Electrochemical Reactions of Pure Indium with Li and Na: Anomalous Electrolyte Decomposition, Benefits of FEC Additive, Phase Transitions and Electrode Performance. *J. Power Sources* **2014**, *248*, 1105−1117.
(37) Okada, K.; Machida, N.; Naito, M.; Shigematsu, T.; Ito, S.; Fujiki, S.; Nakano, M.; Aihara, Y. Preparation and Electrochemical Properties of $LiAlO_2$-Coated $Li(Ni_{1/3}Mn_{1/3}Co_{1/3})O_2$ for All-Solid-State Batteries. *Solid State Ionics* **2014**, *255*, 120−127.
(38) Oh, G.; Hirayama, M.; Kwon, O.; Suzuki, K.; Kanno, R. Bulk-Type All Solid-State Batteries with 5 V Class $LiNi_{0.5}Mn_{1.5}O_4$ Cathode and $Li_{10}GeP_2S_{12}$ Solid Electrolyte. *Chem. Mater.* **2016**, *28*, 2634−2640.
(39) Sakuda, A.; Kitaura, H.; Hayashi, A.; Tadanaga, K.; Tatsumisago, M. Modification of Interface Between $LiCoO_2$ Electrode and $Li_2S-P_2S_5$ Solid Electrolyte Using Li_2O-SiO_2 Glassy Layers. *J. Electrochem. Soc.* **2009**, *156*, A27.
(40) Kim, J.; Kim, M.; Noh, S.; Lee, G.; Shin, D. Enhanced Electrochemical Performance of Surface Modified $LiCoO_2$ for All-Solid-State Lithium Batteries. *Ceram. Int.* **2016**, *42*, 2140−2146.
(41) Levi, M. D.; Salitra, G.; Markovsky Teller, B. H.; Aurbach, D.; Heider, U.; Heider, L. Solid-State Electrochemical Kinetics of Li-Ion Intercalation into $Li_{1-x}CoO_2$: Simultaneous Application of Electroanalytical Techniques SSCV, PITT, and EIS. *J. Electrochem. Soc.* **1999**, *146*, 1279−1289.
(42) Zhang, W. Influence of Surface Area on Thermal Stability of Cathode in Lithium-Ion Battery, Master's Thesis, Technical University of Munich, Ludwigs-Maximilian-University of Munich, University of Augsburg, 2013.
(43) Zhang, W.; Schröder, D.; Arlt, T.; Manke, I.; Pinedo, R.; Weber, D. A.; Sann, J.; Zeier, W. G.; Janek, J. *J. Mater. Chem. A* **2017**, 02730C.
(44) Nobili, F.; Tossici, R.; Marassi, R.; Croce, F.; Scrosati, B. An AC Impedance Spectroscopic Study of Li_xCoO_2 at Different Temperatures. *J. Phys. Chem. B* **2002**, *106*, 3909−3915.
(45) Han, F.; Zhu, Y.; He, X.; Mo, Y.; Wang, C. Electrochemical Stability of $Li_{10}GeP_2S_{12}$ and $Li_7La_3Zr_2O1_2$ Solid Electrolytes. *Adv. Energy Mater.* **2016**, *6*, 1501590.
(46) Sang, L.; Haasch, R. T.; Gewirth, A. A.; Nuzzo, R. G. Evolution at the Solid Electrolyte/Au Electrode Interface during Lithium Deposition and Stripping. *Chem. Mater.* **2017**, *29*, 3029−3037.
(47) Irvine, J. T. S.; Sinclair, D. C.; West, A. R. Electroceramics: Characterization by Impedance Spectroscopy. *Adv. Mater.* **1990**, *2*, 132−138.

DOI: 10.1021/acsami.7b01137
ACS Appl. Mater. Interfaces 2017, 9, 17835−17845

Ningde Amperex Tech. Exhibit No. 2023
Zhuhai CosMX Battery Co. Ltd. v. Ningde Amperex Tech.
IPR2025-00722, U.S. Patent No. 11,799,131
Page 10 of 11

(48) Mizuno, F.; Hayashi, A.; Tadanaga, K.; Tatsumisago, M. Design of Composite Positive Electrode in All-Solid-State Secondary Batteries with Li_2S-P_2S_5 Glass−ceramic Electrolytes. *J. Power Sources* **2005**, *146*, 711−714.
(49) Han, F.; Gao, T.; Zhu, Y.; Gaskell, K. J.; Wang, C. A Battery Made from a Single Material. *Adv. Mater.* **2015**, *27*, 3473−3483.
(50) Okubo, M.; Hosono, E.; Kudo, T.; Zhou, H. S.; Honma, I. Phonon Confinement Effect on Nanocrystalline $LiCoO_2$ Studied with Raman Spectroscopy. *J. Phys. Chem. Solids* **2008**, *69*, 2911−2915.
(51) Park, M.; Zhang, X.; Chung, M.; Less, G. B.; Sastry, A. M. A Review of Conduction Phenomena in Li-Ion Batteries. *J. Power Sources* **2010**, *195*, 7904−7929.
(52) Shin, B. R.; Nam, Y. J.; Oh, D. Y.; Kim, D. H.; Kim, J. W.; Jung, Y. S. Comparative Study of TiS_2/Li-In All-Solid-State Lithium Batteries Using Glass-Ceramic Li_3PS_4 and $Li_{10}GeP_2S_{12}$ Solid Electrolytes (TiS_2). *Electrochim. Acta* **2014**, *146*, 395−402.

DOI: 10.1021/acsami.7b01137
ACS Appl. Mater. Interfaces 2017, 9, 17835−17845

Ningde Amperex Tech. Exhibit No. 2023
Zhuhai CosMX Battery Co. Ltd. v. Ningde Amperex Tech.
IPR2025-00722, U.S. Patent No. 11,799,131
Page 11 of 11